Heterostructured magnetic nanoparticles: their versatility and high performance capabilities

Young-wook Jun, Jin-sil Choi and Jinwoo Cheon*

Received (in Cambridge, UK) 10th October 2006, Accepted 8th November 2006
First published as an Advance Article on the web 11th December 2006
DOI: 10.1039/b614735f

Magnetic nanoparticles exhibit unique nanoscale properties and their utilization for various magnetic systems is of significant interest. Especially, heterostructured magnetic nanoparticles are emerging as next-generation materials due to their synergistically enhanced magnetism and potential multifunctionalities. Herein, we overview the recent advances in the development of magnetic nanoparticles with a focus on multicomponent heterostructured nanoparticles including alloys, core–shells, and binary superlattices synthesized *via* nonhydrolytic methods. Their multifunctionalites and high performance capabilities are demonstrated for applications in high density magnetic storages, chemical catalysis, and biomedical separation and diagnostics.

1 Introduction

The applications of magnetic spins in solid-state materials have enabled significant advances in current informational and biological technologies including information storage, magnetic sensors, bioseparation, and drug delivery. Although micron-sized magnetic materials have been utilized for such purposes,[1–5] researchers are now pursuing further miniaturization of magnetic devices while possessing superior magnetic properties. Magnetic nanoparticles are emerging as a potential candidate for fulfilling such expectations.[6–9] Being different from their bulk counterparts, they exhibit unique nanoscale magnetic behaviors which are highly dependent on morphological parameters such as size and shape.[10–13] Such size and shape effects in nanoparticles enable us the possibility to control their properties (*e.g.* coercivity (H_c) and susceptibility (χ)) as we desire by synthetically tuning their morphological parameters.[11] For example, magnetic nanoparticles possess single domain magnetism below a certain critical size (D_c) where all magnetic spins in the nanoparticle align unidirectionally and therefore bigger nanoparticles give higher magnetic coercivity. (Fig. 1(a)) In comparison, when the size of the particles increases above the critical size ($D > D_c$), multidomain magnetism is observed. Each magnetic domain possesses independent directionality, which results in the decrease of magnetic coercivity. Size-dependent magnetism of Co nanoparticles provides such an example.[13] As the size of the Co nanoparticles increases from 4 to 8 nm, magnetic coercivity at 5 K increases gradually from 370 to 1680 Oe. However, when the size of Co nanoparticles further increases to 10, 12, and 13 nm, the magnetic coercivity decreases to 1600, 1100, and 250 Oe (Fig. 1(b)). This result indicates that the critical single domain size of Co nanoparticles is around 8–10 nm.

During the past decade, various synthetic methods for producing magnetic nanoparticles have been studied including chemical vapor deposition (CVD),[14–16] powder pyrolysis,[17,18] and liquid-phase colloidal synthesis in aqueous[19–26] or nonhydrolytic[27–72] medium. Among them, the liquid phase

Department of Chemistry, Yonsei University, Seoul, 120-749, Korea. E-mail: jcheon@yonsei.ac.kr

Young-wook Jun

Young-wook Jun earned his BS degree in chemistry from Yonsei University (1999) and his PhD degree in chemistry from the Korea Advanced Institute of Science and Technology (KAIST) (2005). Currently, he is carrying out postdoctoral studies as a member of Professor Cheon's group at Yonsei University. He is a recipient of the Honorable Mention Award of the IUPAC Prize for Young Chemists (2005). His current research focuses on the development of smart inorganic nanocrystal–biomolecule hybrid systems for biomedical imaging and sensor applications.

Jin-sil Choi

Jin-sil Choi was born in 1980 in Daegu, Korea. She received her BS degree in chemistry from Yonsei University in 2004 and now is a third year graduate student pursuing her PhD degree at Yonsei University under the supervision of Prof. Jinwoo Cheon. She is a recipient of the Seoul Science Fellowship (2006). Her current research interests are the fabrication of shape, size and composition controlled multicomponent inorganic nanocrystals and their biocompatibility and safety evaluation in biological systems.

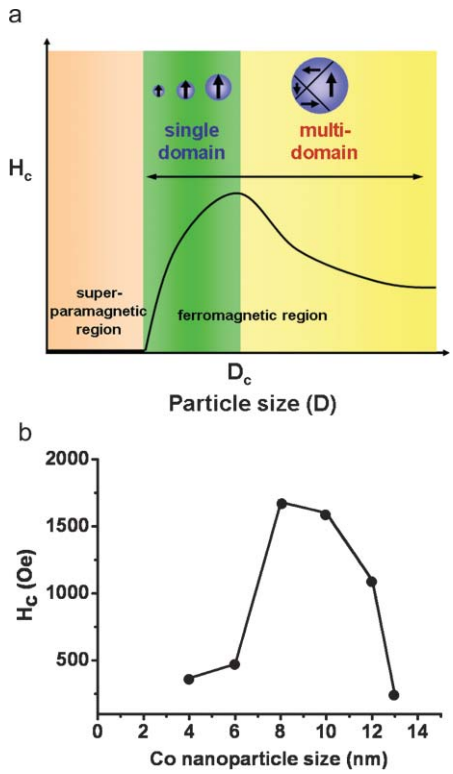

Fig. 1 Magnetism of nanoparticles. (a) A plot of magnetic coercivity (H_c) *vs.* size.[11] (b) Experimental size-dependent magnetic coercivity of Co nanoparticles.[13]

Jinwoo Cheon

Jinwoo Cheon is a Professor of Chemistry at Yonsei University and Head of the Nanomaterials Division of the Nano-Medical National Core Research Center of Korea. He received his BS and MS degrees in chemistry from Yonsei University in Seoul, Korea. He then moved to the University of Illinois, Urbana-Champaign where he earned his PhD in organometallics and materials chemistry from Prof. G. Girolami in 1993. After receiving post-doctoral training at the U.C. Berkeley, and also at UCLA, he joined the Korea Advanced Institute of Science and Technology (KAIST) as an assistant professor in 1998. In 2002, he moved to Yonsei University. Professor Cheon was elected as a junior member of the Korean Academy of Science and Technology (2003) and is a recipient of the Yonsei Research Achievement Award (2006), the Korean Chemical Society Award in Inorganic Chemistry (2004), the National Science Prize for Junior Faculty (2002), and the Korean Chemical Society-Wiley Young Chemist Award (2001). His research areas include the synthetic chemistry of inorganic nanocrystals, nanoscale biomagnetics and the applications of nanomaterials for biomedical sciences.

colloidal synthetic approach is an especially powerful tool for the convenient and reproducible synthesis of magnetic nanoparticles. Previously, nanoparticles were generally grown in aqueous media by chemical reactions of precursor molecules in the presence of structured micelles at room temperature.[19–26] However, nanoparticles obtained by this method frequently suffer from relatively poor crystallinity or polydispersity in their size and shape, which adversely influences their magnetism.[21,25] More recently, nonhydrolytic synthetic approaches have been developed to overcome some of these problems. This method not only produces highly crystalline and monodispersed spherical magnetic nanoparticles but also enables the fabrication of more complex heterostructured nanoparticles such as magnetic alloys,[27–33] core–shells and onions,[28,34–39] and dimers and multimers.[40–48]

Further technological advancements require rational assembly and hybridization of these magnetic nanoparticles with other components such as chemical and biological molecules so that one can utilize them as key components for the fabrication of high performance magnetic nanosystems with chemical, electronic and biological applications. These include ultrahigh density magnetic storage media,[27,73,74] chemical catalysis and separation,[33,75] magnetic vectors and probes for bioseparation,[76–81] biosensing,[82–85] and molecular imaging[86–90] (Fig. 2).

In this feature article, we limit our scope to the representative aspects in recent progresses of nonhydrolytically synthesized magnetic nanoparticles and their various areas of utilization. First, we describe representative studies for the nonhydrolytic fabrication of magnetic nanoparticles with a focus on alloys, core–shells, and magnetic binary superlattices. New phenomena associated with these heterostructured magnetic nanoparticles are briefly described. Also, we discuss versatile utilizations of such magnetic nanoparticles for technologically important applications as illustrated in Fig. 2.

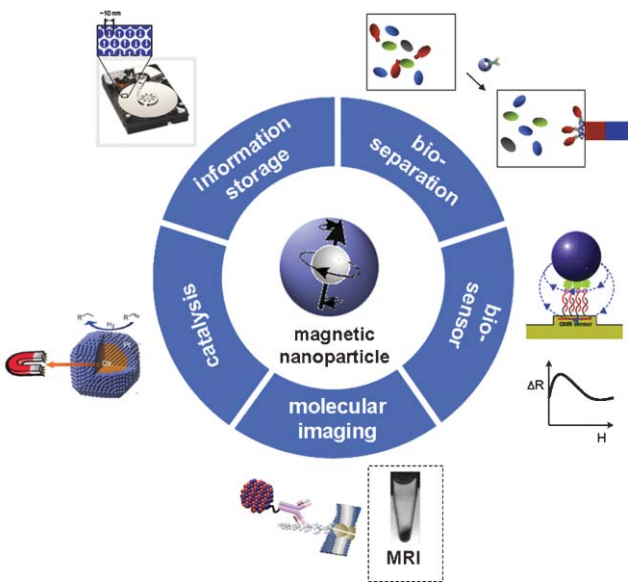

Fig. 2 Applications of magnetic nanoparticles for high-performance nanosystems.

2 Nonhydrolytic colloidal synthesis of magnetic nanoparticles

2.1 Monometallic magnetic nanoparticles and their oxides

In earlier studies, researchers have extensively explored the synthesis of monometallic magnetic nanoparticles such as cobalt,[13,49–51] iron,[52–55] nickel,[56–60] and the oxides of these metals.[61–72] Those are well reviewed previously,[53,63,71] and in this article we just expose limited glances of them. For example, Sun and Murray reported that the reduction of $CoCl_2$ by lithium triethylborohydride in a hot organic solution with surfactant molecules including trialkylphosphine and a long chain alkyl acid induces the formation of highly monodispersed cobalt nanoparticle spheres with controllable size (Fig. 3).[49] Anisotropic shapes of magnetic Co, Ni and Fe nanoparticles such as rods,[58,60] discs,[13,50] and cubes[57,72] could be synthesized by controlling parameters such as the type of surfactant molecule, growth time and growth temperature. Syntheses of magnetic metal oxide nanoparticles have also been extensively studied. For example, Peng, Hyeon, and others reported the synthesis of monodispersed magnetic metal oxide nanoparticles by thermolysis of metal fatty acid precursors.[61,62] Sun *et al.* proposed a highly size-controllable magnetic metal ferrite nanoparticle synthesis utilizing Lamor growth on smaller nanoparticle seeds.[64] Cheon *et al.* showed that shape control of iron oxide nanoparticles was possible.[65] Thermal decomposition of $Fe(CO)_5$ under aerobic conditions resulted in various shapes of γ-Fe_2O_3 nanoparticles including triangles, diamonds and hexagons.

2.2 Multicomponent heterostructured magnetic nanoparticles: "solid-solution" and "core–shell" type nanoparticles

The magnetic and chemical properties of monometallic elements are known to be significantly enhanced by the formation of alloys with additional heterometals which can provide many advantages such as high magnetic anisotropy, enhanced magnetic susceptibility, and large coercivity.[10–12] Such alloy effects in colloidal nanoparticle systems have been demonstrated by Murray, Sun, and co-workers in the synthesis of "solid solution" FePt (Fig. 4(a)).[27] It is known that the reduction of $Pt(acac)_2$ (acac = acetylacetonate) by a diol produces Pt metal and thermal decomposition of $Fe(CO)_5$ in high-temperature solution results in the formation of Fe particles. They reported that when both chemical reactions are initiated together in the presence of oleic acid and oleylamine, monodispersed FePt nanoparticles are formed. The relative composition of these FePt nanoparticles is shown to be readily adjusted by controlling the molar ratio of $Fe(CO)_5$ to $Pt(acac)_2$ between $\sim$7 : 3 to $\sim$3 : 7, *via* $\sim$1 : 1. As-synthesized FePt nanoparticles are of a face-centered cubic (fcc) structure and possess superparamagnetic behavior at room temperature. However, they found that these fcc-FePt nanoparticles can be transformed into ferromagnetic a face-centered tetragonal (fct) structure with a significantly enhanced magnetism coercivity of $\sim$5000 Oe upon thermal annealing at 600 °C (Fig. 4(b)–(g)). Furthermore, the annealed fct-FePt nanoparticle assemblies are smooth ferromagnetic films that can serve as high-density magnetization reversal transitions (bits).

Magnetic $CoPt_3$ solid-solution nanoalloys can be synthesized through a similar strategy. Weller and co-workers reported that thermal decomposition of $Co_2(CO)_8$ and reduction of $Pt(acac)_2$ in the presence of 1-adamantanecarboxylic acid produce monodispersed, highly crystalline $CoPt_3$

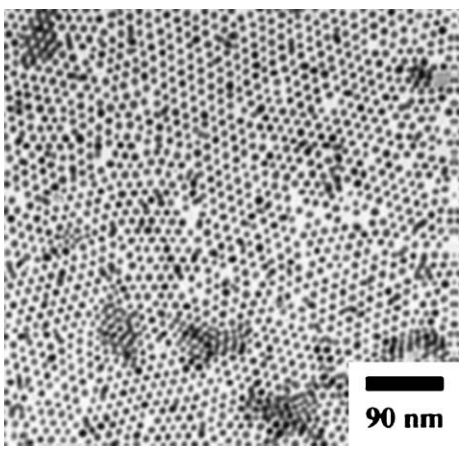

Fig. 3 Transmission electron microscopic (TEM) image of 9 nm Co nanoparticles synthesized through the thermal decomposition of $CoCl_2$ in a mixture of oleic acid and tributylphosphine surfactants.[49]

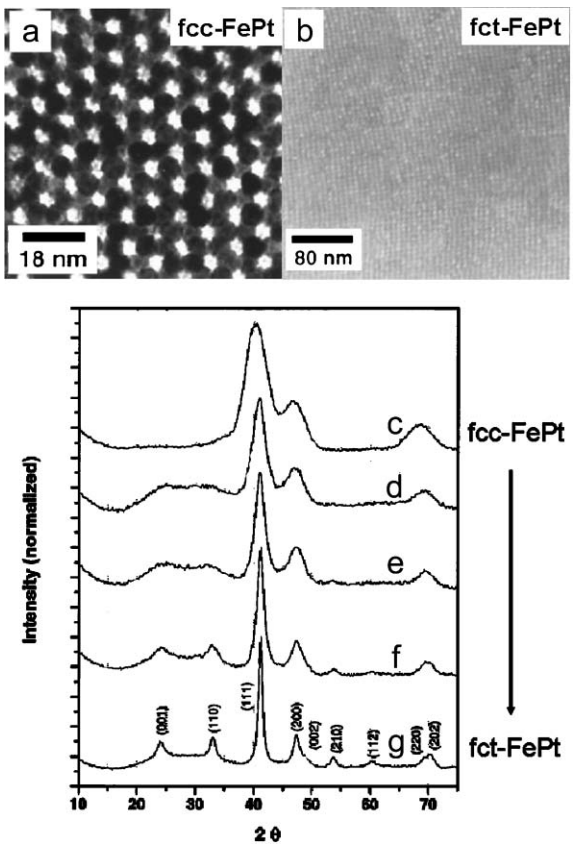

Fig. 4 (a) TEM image of as-synthesized fcc-FePt nanoparticle superlattices. (b) Scanning electron microscopic (SEM) image and high-resolution TEM (HRTEM, inset) image of fct-FePt after thermal annealing processes. (c)–(g) X-Ray diffractometric (XRD) monitoring of phase transition from fcc-FePt to fct-FePt. (c) As-synthesized fcc-FePt, (d)–(g) FePt annealed at 450, 500, 550, and 600 °C.[27]

nanoparticles.[30] The mean particle size can be varied from 1.5 to 7.2 nm by controlling the reaction conditions and the type of surfactants (Fig. 5). As-synthesized $CoPt_3$ particles represent single crystal domains and have a chemically disordered fcc structure.

Thermally induced co-reduction of two different kinds of metal ion complexes can also be utilized for magnetic nanoalloy synthesis. Hyeon and co-workers synthesized NiPd nanoalloys through thermal decomposition of trioctylphosphine (TOP) adducts of $Ni(acac)_2$ and $Pd(acac)_2$ in a hot mixture of TOP and oleylamine surfactants.[33] Since the Ni-TOP adducts decompose at relatively lower temperatures compared to Pd-TOP adducts, it was possible to fabricate NiPd nanoalloys with graded Pd composition by tuning the growth temperature of the nanoparticles (Fig. 6). The inner region of the alloy is composed of Ni-rich NiPd, while the outer region of the alloy possesses a Pd-rich structure. NiPd nanoalloys can be utilized as an efficient catalyst for Sonogashira coupling reactions.

Sequential decomposition of molecular precursors can be effective for the synthesis of core–shell type heterostructured nanoparticles. Yang and co-workers reported that $Pt_{core}(Fe_2O_3)_{shell}$ nanoparticles can be obtained by the sequential decomposition of $Pt(acac)_2$ and $Fe(CO)_5$ (Fig. 7(a)).[36] A thermally induced alloying effect of these core–shell nanoparticles to form solid solution fct FePt nanoalloys was clearly observed.[31] Sun and co-workers have utilized a similar strategy to produce $(FePt)_{core}(Fe_3O_4)_{shell}$ nanoparticles.[38] They first synthesized FePt seeds and, after isolation, Fe_3O_4 shells were further grown by thermal decomposition of $Fe(acac)_3$ in the presence of alkyldiol reductants and surfactant molecules. They extended this protocol for the fabrication of $(CoFe)_{core}(Fe_3O_4)_{shell}$ by utilizing CoFe seeds (Fig. 7(b)).[39] Klimov and co-workers reported that this sequential decomposition method could be applicable for the synthesis of $Co_{core}(CdSe)_{shell}$ nanoparticles

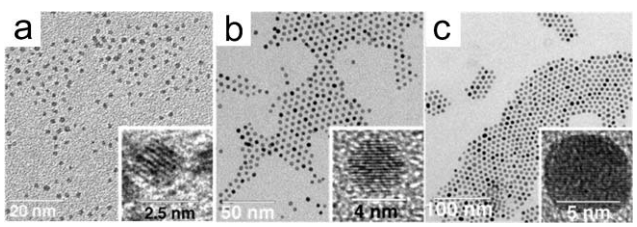

Fig. 5 TEM images of various sizes of solid-solution $CoPt_3$ nanoparticles: (a) 1.5 nm, (b) 4 nm, and (c) 6 nm.[30]

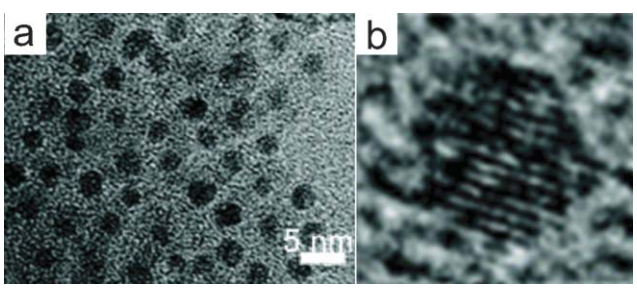

Fig. 6 (a) TEM image and (b) HRTEM images of NiPd nanoalloys.[33]

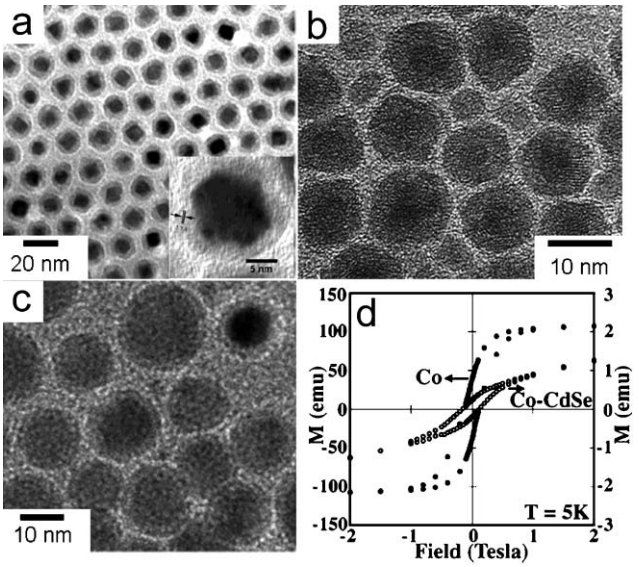

Fig. 7 (a) TEM and HRTEM (inset) images of $Pt_{core}(Fe_2O_3)_{shell}$.[36] (b) TEM image of $(CoFe)_{core}(Fe_3O_4)_{shell}$ nanoparticles.[39] (c) TEM image of $Co_{core}(CdSe)_{shell}$ nanoparticles. (d) Hysteresis loops of Co seed and $Co_{core}(CdSe)_{shell}$ nanoparticles.[37]

(Fig. 7(c)).[37] They further demonstrated that these heterostructured nanoparticles exhibit bifunctional properties of magnetism and optical fluorescence. The magnetic coercivity of $Co_{core}(CdSe)_{shell}$ was almost identical to that of Co seed nanoparticles (Fig. 7(d)). In the optical spectra, large Stokes shift was observed from $Co_{core}(CdSe)_{shell}$ nanoparticles compared with similar sized CdSe nanoparticles due to shape anisotropy of the CdSe shell.

Although the above-mentioned co-decomposition and sequential decomposition methods have been utilized for solid solution and core–shell nanoparticle synthesis, in some cases, these methods can result in undesired nucleation and inhomogeneous particle growth. In order to avoid such problems, Cheon and co-workers adopted a redox transmetalation strategy to effectively synthesize bimetallic magnetic nanoalloys (Fig. 8). They utilized $Co_2(CO)_8$ as the Co precursor and $Pt(hfac)_2$ (hfac = 1,1,1,5,5,5-hexafluoro-2,4-pentadionate) as the Pt precursor.[28] The formation of CoPt nanoalloys is driven by redox transmetalation reactions between thermally decomposed Co clusters and the Pt(II) precursor, where Pt(II) is reduced to Pt(0) at the expense of the sacrificial oxidation of Co(0) to Co(II) due to the positive electrochemical potential of the redox reaction (Fig. 8(a), (c), eqn (1)). In this case, the reaction proceeds spontaneously without the need for any additional reductants (*e.g.* diol). By tuning the ratio of Co and Pt precursors, control of the stoichiometric composition of CoPt nanoalloys is also possible from Co_1Pt_1 to Co_1Pt_3.

$$Co^0 + Pt^{2+} \rightarrow Co^{2+} + Pt^0; \quad E^\circ = 1.46\ V \qquad (1)$$

This redox transmetalation strategy can be especially useful for the synthesis of core–shell CoPt nanoparticles. When Co nanoparticles were used to react with $Pt(hfac)_2$, redox transmetalation between the surfacial Co atoms and

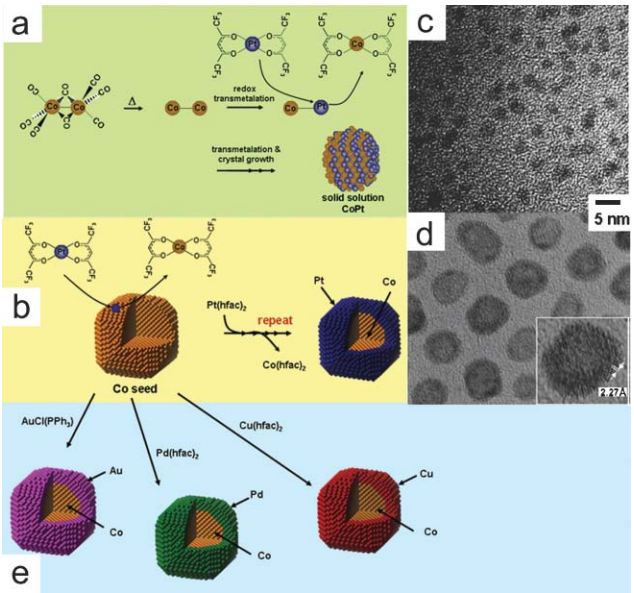

Fig. 8 Schematics of transmetalation processes for (a) solid solution and (b) core–shell nanoparticles. TEM image of (c) solid solution $CoPt_3$ and (d) core–shell $Co_{core}Pt_{shell}$ nanoparticles.[28] (e) Generalization of redox transmetalation processes for the fabrication of $Co_{core}Au_{shell}$, $Co_{core}Pd_{shell}$, and $Co_{core}Cu_{shell}$ nanoparticles.[34]

$Pt(hfac)_2$ induced selective growth of a Pt shell around a Co nanoparticle core, which finally resulted in the formation of $Co_{core}Pt_{shell}$ nanoparticles (Fig. 8(b), (d), eqn (2)).

$$Co_m(\text{nanoparticle}) + n\ Pt(hfac)_2 \rightarrow (Co_{m-n})_{core}Pt_{shell} + n\ Co(hfac)_2 \quad (2)$$

They showed that the redox transmetalation strategy is versatile for the fabrication of core–shell magnetic nanoparticles including $Co_{core}Au_{shell}$, $Co_{core}Pd_{shell}$, and $Co_{core}Cu_{shell}$ (Fig. 8(e)).[34] In addition, it was also found that these core–shell type CoPt nanoparticles are easily transformed into ferromagnetic solid solution fct-CoPt nanoalloys after thermal annealing processes at 700 °C (Fig. 9(a), (b)).[32] The effect of the structural phase transition on the magnetic properties is critical. Although $Co_{core}Pt_{shell}$ nanoparticles show superparamagnetism with zero magnetic coercivity (H_c = 0), the samples annealed at 700 °C show ferromagnetism with a H_c of 5300 Oe at room temperature (Fig. 9(c), (d)). The annealed CoPt nanoparticles retain their size (6 nm) without forming bulk CoPt and are observed to be nanoscale ferromagnets which can potentially be used as magnetic bits for tera-level information storage applications.

2.3 Binary magnetic superlattices

Another strategy for the fabrication of heterostructured magnetic nanostructures is to co-assemble various magnetic nanoparticles into ordered superlattices. When nanoparticles form a close packed superlattice, two interstitial sites are generated: One is an octahedral site (O_h) and the other is a tetrahedral (T_d) site. Filling these void sites with a different kind of magnetic nanoparticles results in the formation of binary magnetic superlattices (Fig. 10). Such binary magnetic

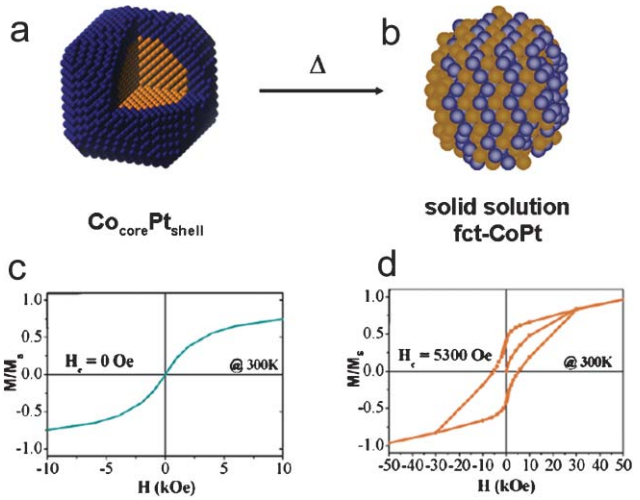

Fig. 9 (a, b) Schematic of phase transition of $Co_{core}Pt_{shell}$ nanoparticles to solid solution fct-CoPt nanoparticles. Hysteresis loops of (c) $Co_{core}Pt_{shell}$ nanoparticles and (d) solid solution fct-CoPt.[32]

superlattices allow them to have novel magnetic functionalities. For example, its close packed structure can promote interesting nanoscale chemical reactions or magnetic couplings between two nanoparticle constituents.

Binary magnetic assemblies of FePt and Fe_3O_4 provide such an example.[91] Sun and co-workers fabricated three-dimensional binary assemblies through the slow evaporation of hexane containing both FePt and Fe_3O_4 nanoparticles resulting in randomly mixed or locally arranged binary assemblies in which each Fe_3O_4 nanoparticle is surrounded by 6–8 FePt nanoparticles (Fig. 11(a)). Upon the annealing process of FePt–Fe_3O_4 binary assemblies under an Ar–H_2 atmosphere, the fcc-FePt nanoparticles are converted into fct-FePt, while the Fe_3Pt phase is also formed around the FePt phase by reduction of Fe_3O_4 to Fe and partial interdiffusion between Fe and FePt (Fig. 11(b)). Originally, these two phases can exhibit different magnetic properties: fct-FePt considered as a magnetically hard phase with high magnetocrystalline anisotropy and Fe_3Pt considered as a magnetically soft phase.

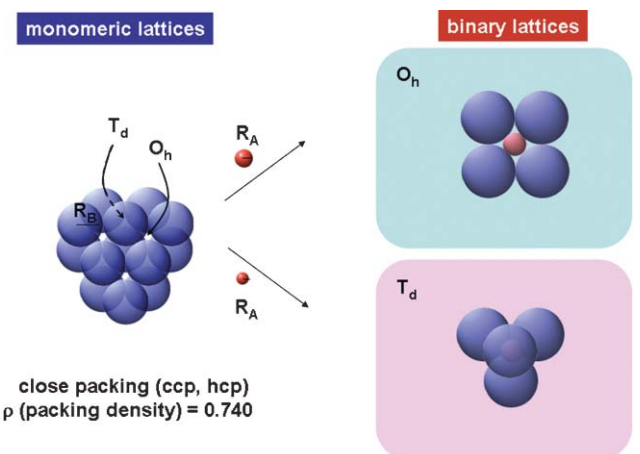

Fig. 10 Schematic of the formation of binary superlattices from monomeric superlattices by filling void O_h and T_d holes with smaller nanoparticles (red).

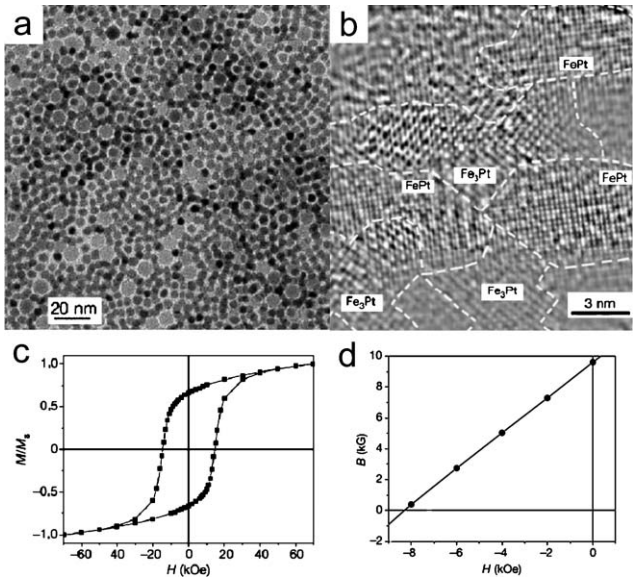

Fig. 11 (a) Binary assemblies of 4 nm FePt and 8 nm Fe_3O_4. (b) HR-TEM image of Fe_3Pt–FePt exchange coupled magnets fabricated by thermal annealing of 4 nm FePt and 8 nm Fe_3O_4. (c) Hysteresis loop and (d) BH curve of Fe_3Pt–FePt exchange coupled magnets.[91]

However, the hysteresis measurement shows that the magnetization changes smoothly in the presence of an external magnetic field, which is similar to the hysteresis behaviour of a single-phase material, due to hard–soft exchange coupling between the two phases (Fig. 11(c)). Systematically controlling the mass ratio of FePt : Fe_3O_4 in the initial assembly results in a highly enhanced energy product $(BH)_{max}$ of 20.1 MG Oe, which exceeds the theoretical limit of 13 MG Oe for nonexchange coupled FePt (Fig. 11(d)).

Another interesting magnetic phenomenon was observed in the binary assemblies of Co and Fe_3O_4, reported by Cheon *et al.*[92] They initially co-assembled these two different types of magnetic nanoparticles into three-dimensional superlattices by controlling the particle size ratio and stoichiometric composition to form either AB or AB_2 depending on assembly procedures (Fig. 12). Since each Fe_3O_4 nanoparticle is surrounded by a highly symmetric arrangement of Co nanoparticles within a distance of about one nanometer in this superlattice, nanoscale chemical and physical interactions between these two nanoparticles can be exploited to generate unique phase transitional behaviors. When the binary superlattices were thermally annealed at elevated temperatures, the

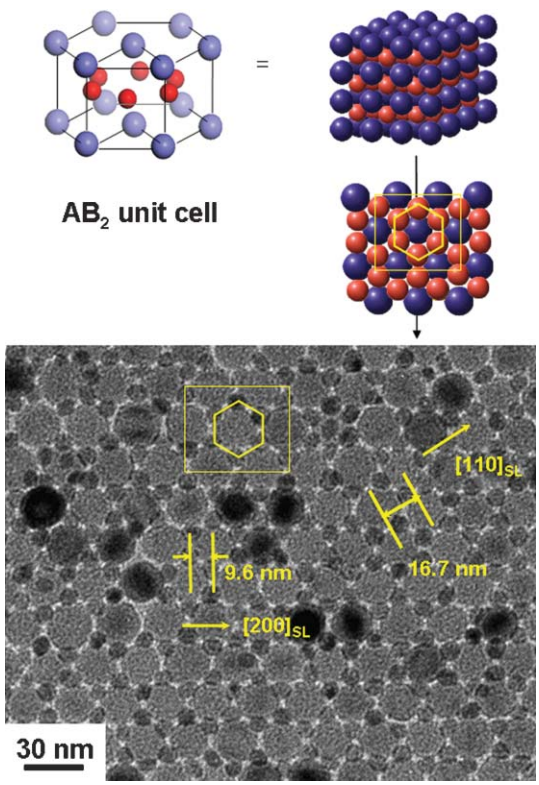

Fig. 12 Schematic of unit cell and TEM image of AB_2 type binary superlattice. 18 nm Fe_3O_4 nanoparticles form a hexagonally close-packed layer, and 7.5 nm Co nanoparticles form a second layer, which are situated in the interstices of Fe_3O_4 layers.[92]

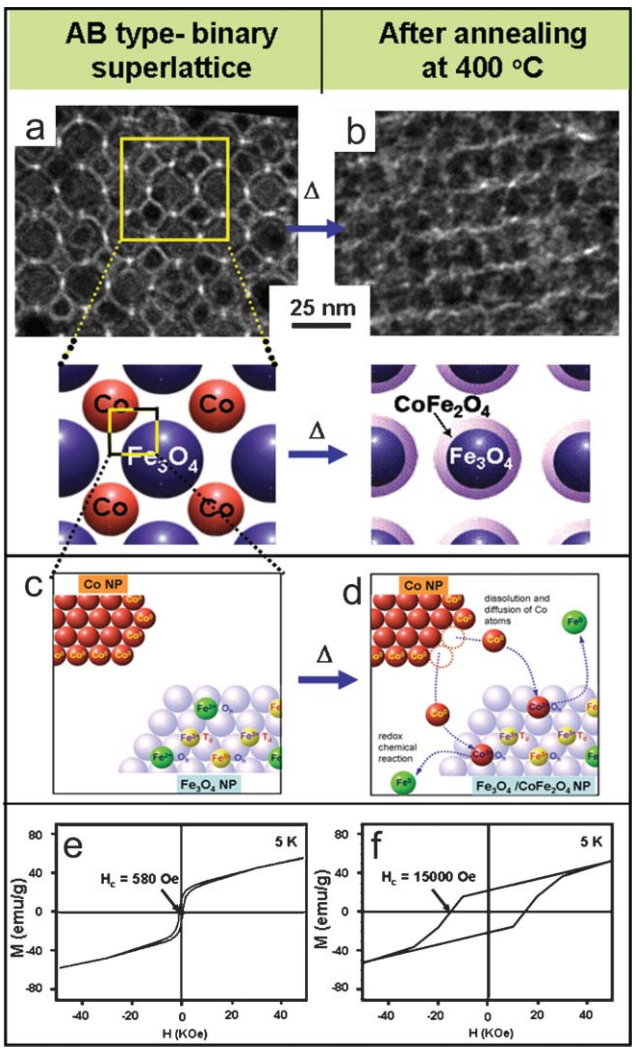

Fig. 13 Ferromagnetic phase transition from binary superlattices of Co and Fe_3O_4 to $(Fe_3O_4)_{core}(CoFe_2O_4)_{shell}$ superlattices. (a, b) TEM images. (c, d) Redox chemical reactions between Co nanoparticles and Fe_3O_4 nanoparticles. (e, f) Hysteresis loops of binary and core–shell superlattices, respectively.[92]

nanoscale transformation of as-assembled binary superlattices of Fe_3O_4 and Co nanoparticles into $(Fe_3O_4)_{core}(CoFe_2O_4)_{shell}$ superlattices was driven through intra-superlattice redox chemical processes (Fig. 13(a)–(d)): the transformation processes involve (i) dissolution and diffusion of Co atoms from Co nanoparticles into a Fe_3O_4 inverse spinel matrix, and (ii) alloying of Co and Fe_3O_4 by the exchange of Fe^{2+} occupying an O_h site with a Co atom through redox chemical reactions in which a Co atom is oxidized at the expense of an Fe^{2+}. Such $(Fe_3O_4)_{core}(CoFe_2O_4)_{shell}$ superlattice formation leads to significant changes in magnetism. As-assembled AB type superlattices have magnetic coercivity value of 580 Oe at 5 K (Fig. 13(e)), which is roughly in between the values for individual Co (780 Oe) and Fe_3O_4 (200 Oe) nanoparticles. After thermal annealing processes at 400 °C, however, the magnetic coercivity of AB structures increases to 15000 Oe (about 25 times higher than the initial value) (Fig. 13(f)). Since such dramatic magnetic enhancement is not observed for phase segregated binary assemblies of Fe_3O_4 and Co nanoparticles, it is suggested that the symmetry and proximity effects between the two nanoparticle components are essential in observing such nanoscale magnetic phenomena.

3 Versatile applications of heterostructured magnetic nanoparticles for high-performance applications

3.1 Magnetic recording media

The primary application of magnetic nanoparticles is for use in magnetic recording media. Although micron- or sub-micron-sized magnetic materials have been used for such purposes to date, magnetic nanoparticles are now emerging for the realization of ultrahigh density tera-level storage media due to their unique single domain magnetism and very small size. For example, the fct-FePt superlattices, described in Section 2.2, can be fabricated as smooth ferromagnetic films for high-density bits.[27] When a ~120 nm thick assembly of 4 nm FePt nanoparticles with in-plane coercivity of 1800 Oe was tested for the initial recording experiments, a clear magneto-resistive read-back sensor voltage signal from the written data tracks was obtained up to a linear density of 5000 flux changes per millimeter (fc mm^{-1}) (Fig. 14). Although the initial result is below the value for the highest currently achievable linear density of ~20000 fc mm^{-1}, much higher recording densities can be expected if the thickness of the FePt ferromagnetic superlattices can be reduced to near monolayer levels.

3.2 Dual-functional core–shell nanoparticles for catalysis and magnetic separation

Since nanoparticles possess high surface-to-volume ratio and their electronic structures can be modulated by their size, shape, and composition, their utilization as catalysts in organic reaction is also of interest. Earlier attempts have mainly focused on the development of monometallic nanoparticle catalysts for highly efficient organic reactions. Researchers are now beginning to utilize bimetallic nanoparticles in order to improve their catalytic activity by modifying the electronic and surface properties. Such bimetallic nanoparticle catalytic systems are "atomically economical" because precious

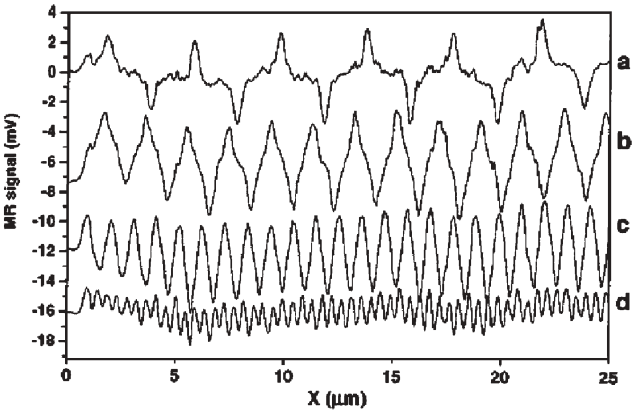

Fig. 14 Magneto-resistive read-back signals from written bit transitions in a 120 nm thick assembly of 4 nm $Fe_{48}Pt_{52}$ nanoparticles. The individual line scans reveal magnetization reversal transitions at linear densities of (a) 500 fc mm^{-1}, (b) 1040 fc mm^{-1}, (c) 2140 fc mm^{-1} and (d) 5000 fc mm^{-1}.[27]

catalytic metals such as Rh, Pt and Pd can be conserved by replacing the interior of the nanoparticles with inexpensive core metal. For example, NiPd bimetallic nanoalloys described in Section 2.2 was successfully utilized for Sonogashira

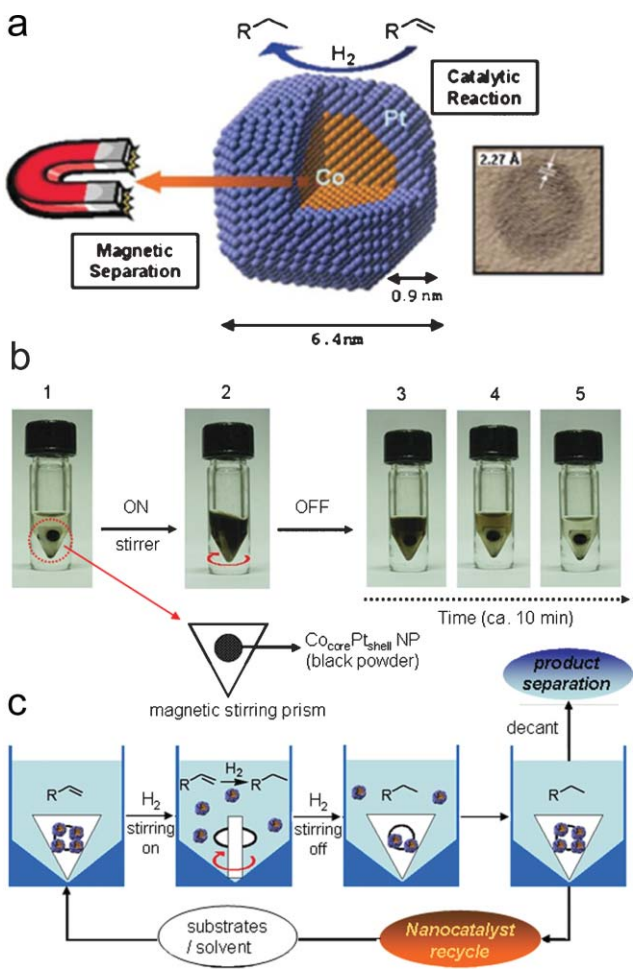

Fig. 15 (a) Schematic of magnetic and catalytic $Co_{core}Pt_{shell}$ nanoparticles. (b, c) Magnetic auto-recycling of $Co_{core}Pt_{shell}$ catalyst.[75]

Table 1 Catalytic hydrogenation of 1-decene by $Co_{core}Pt_{shell}$ nanoparticles with catalyst recycling[a]

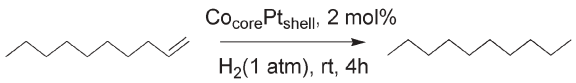

Run	Yield[b] (%)	Run	Yield[b] (%)
1	100	5	100
2	100	6	100
3	100	7	100
4	100		

[a] *Reaction conditions*: Substrate: 0.25 mmol, 1-decene/Pt atom = 50 (2 mol%), toluene: 0.1 ml, 1 atm H_2 (using toy balloon), room temperature. [b] Determined by GC and GC-MS.

coupling reaction between aryl halide and alkyne molecules (eqn (3)).[33]

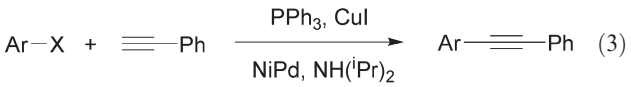

(3)

In addition to improving catalytic activity, bimetallic magnetic nanoparticles can have genuine dual-functionalities due to the presence of two nanoparticle components. For example, $Co_{core}Pt_{shell}$ nanoparticles exhibit both catalytic activity due to its Pt shell and convenient separation and recycling of the nano-catalysts due to the superparamagnetism of its Co core (Fig. 15(a)).[75] When these core–shell nanoparticles were tested in the hydrogenation of 1-decene under a H_2 atmosphere, its complete conversion to *n*-decane was observed. After the reaction completed, the catalyst recycled itself by magnetic auto-separation. Initially, all black colored $Co_{core}Pt_{shell}$ nanoparticles collected onto the central part of a magnetic stirring bar due to magnetic attraction. However, once the movement of the magnetic stir bar is initiated, the nanoparticles are fully dispersed by centrifugal force, giving rise to the desired nano-catalytic hydrogenation reaction (Fig. 15(b), (c)). The nanoparticles retained their excellent catalytic activity compared to that of freshly prepared nanoparticles after up to seven cycles (Table 1).

3.3 Magnetic nanoparticles for bio-medical separation and diagnostics

Due to their small size, comparable to biological functional units, and their unique nanoscale magnetic properties, magnetic nanoparticles are highly effective as important probes and vectors for biomedical separation,[76–81] diagnosis,[86–90] and therapy.[93,94] For example, the utilization of magnetic attraction between magnetic particles and external magnets enables separation of biomolecules such as proteins,[77–79] bacteria[76] and cells.[80,81] Although mainly micron-sized magnetic beads have been previously used for such purposes, researchers are now utilizing smaller-sized nanoparticles which can provide high colloidal stability, optimized target-specificity, minimal nonspecific binding, and enhanced magnetic behaviors. Xu and co-workers utilized FePt nanoparticles for bacteria separation.[76] For this purpose, they first nonhydrolytically synthesized FePt nanoparticles. The surface ligands were then exchanged with thiol modified vancomycin which has the ability to specifically recognize the

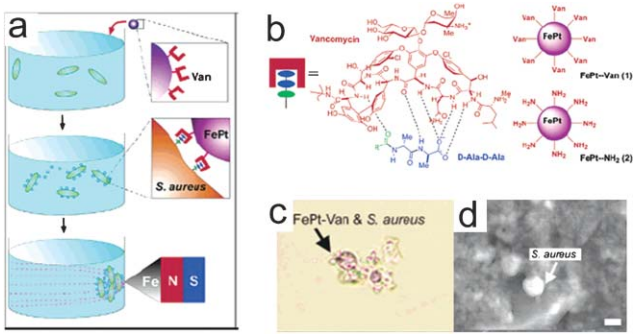

Fig. 16 Magnetic separation of bacteria using vancomycin-coated FePt nanoparticles. (a) Schematic of magnetic separation procedures. (b) Bio-recognition of vancomycin and D-Ala-Ala terminal peptide. (c, d) Optical and SEM images of magnetically separated bacteria.[76]

terminal D-Ala-Ala peptide region located in the cell wall of Gram-positive bacteria *via* hydrogen bonding. The magnetic nanoparticle–vancomycine conjugates selectively captured the target bacteria through vancomycin–D-Ala-Ala interactions (Fig. 16) and were separated by an external magnet. They utilized a similar strategy for the separation of histidine-tagged protein by utilizing nickel nitrilotriacetic acid (NTA) coated $Co_{core}(Fe_2O_3)_{shell}$ nanoparticles.[77] Hyeon and co-workers studied another type of imidazole-coated $Ni_{core}NiO_{shell}$ nanoparticle for the separation of a histidine-tagged protein.[78] Since it is known that histidine strongly binds to nickel(II), the histidine-tagged protein is readily captured by the nanoparticle. The superparamagnetic property of the Ni core allows for the collection of the histidine-tagged protein coated nanoparticles by an external magnet (Fig. 17).[78]

Magnetic nanoparticles can be effective as magnetic probes for magnetoresistance biosensors.[82,83] Although micron-sized magnetic beads have been widely used as probes previously, their magnetic inhomogeneity and potential nonspecific binding have posed problems. In addition, they tend to block selective biomolecular interactions with limited sensitivity.

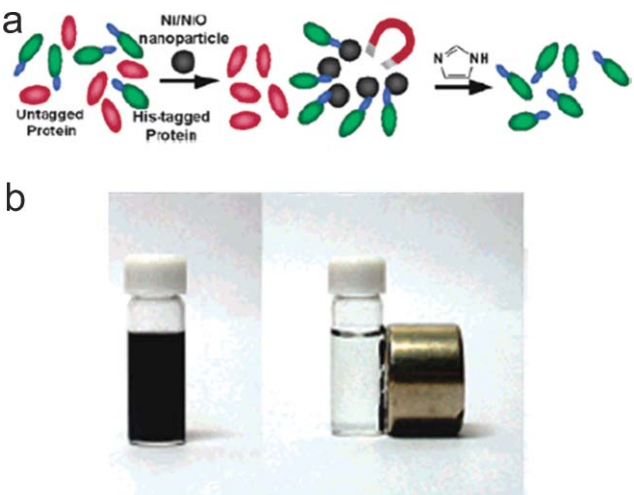

Fig. 17 Magnetic separation of histidine-tagged proteins by using $Ni_{core}NiO_{shell}$ nanoparticles. (a) Schematic and (b) magnetic separation.[78]

Held and co-workers nicely utilized manganese ferrite nanoparticles ($MnFe_2O_4$) for magnetic tunnel junction (MTJ) biosensors.[83] When biotin-coated $MnFe_2O_4$ nanoparticles were incubated in the avidin-patterned MTJ substrate, a change in the magnetoresistance signal was clearly observed due to the selective nanoparticle binding of the substrate (Fig. 18).

Another attractive biomedical application of magnetic nanoparticles is to utilize them as next generation imaging probes for observing biological events *via* magnetic resonance imaging (MRI).[86–90] MRI is one of the most powerful medical diagnostic tools due to its noninvasive nature and multi-dimensional tomographic capabilities coupled with high spatial resolution. Although MRI lags in sensitivity when compared with other diagnostic tools, such weakness can be significantly improved by using magnetic nanoparticles. Under an applied magnetic field, these nanoparticles become magnetized and generate induced magnetic fields, which can perturb the magnetic relaxation processes of the protons in the surrounding water molecules. This phenomenon leads to the shortening of the spin–spin relaxation time ($T2$) of the proton, which results in darkening of MR images (Fig. 19). By using such MR contrast effects of magnetic nanoparticles as probes, it is possible to observe molecular events in biological systems.

For the success of molecular MR imaging, it is necessary to have highly well-defined magnetic nanoparticles which exhibit excellent magnetic properties, the ability to escape from the reticuoendothelial system (RES), and the possession of active functionality that can be linked with biologically active molecules. Fortunately, nonhydrolytic high-temperature growth methods can allow one to have size-controllability, high single crystallinity, and good stoichiometry. Cheon, Suh,

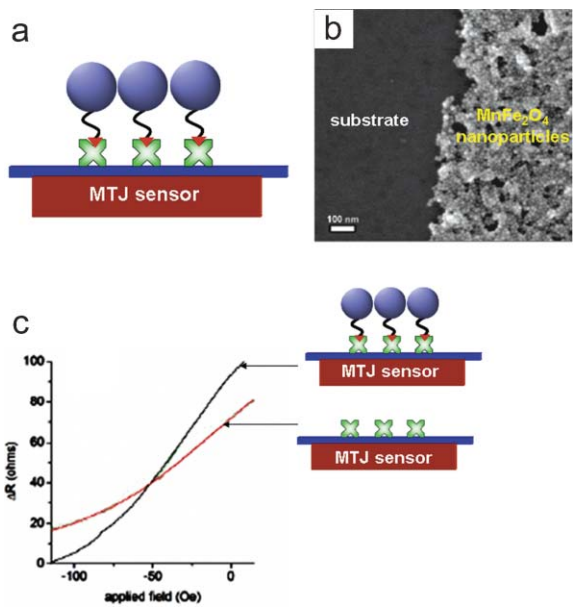

Fig. 18 (a) $MnFe_2O_4$ nanoparticle based magnetoresistance-magnetic tunneling junction (MTJ) sensors for the detection of avidin–biotin interaction. (b) Scanning electron microscopic image of $MnFe_2O_4$ nanoparticles bound to the avidin-patterned region of substrate. (c) Magnetoresistance measurement taken before (red line) and after (black line) the binding of biotin-coated nanoparticles.[83]

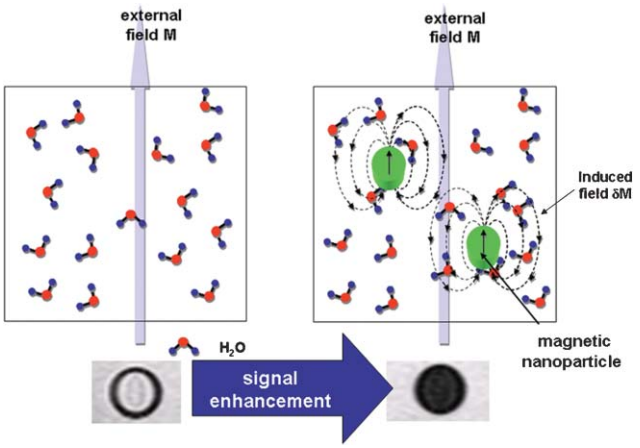

Fig. 19 Magnetic contrast effect of magnetic nanoparticles in water. Induced magnetic field by magnetic nanoparticles perturbs the magnetic relaxation processes of the protons in water molecules, which results in the shortening of $T2$ of the proton with a dark MR contrast.

and co-workers demonstrated such advantages of nonhydrolytically synthesized iron oxide nanoparticles in applications as MR contrast agents.[88,89] As shown in the TEM image (Fig. 20), nanoparticles obtained are highly monodispersed spheres ($\varepsilon < 8\%$). HRTEM and X-ray analyses show that the nanoparticles are single crystalline stoichiometric Fe_3O_4. Water-soluble iron oxide nanoparticles (WSIO) are attained by introducing the 2,3-dimercaptosuccinic acid (DMSA) ligand onto the nanoparticle surface. When these nanoparticles are conjugated with herceptin, they successfully detect cancer cells (SK-BR-3) as a dark MR image resulting from molecular interactions between the nanoparticle surface-bound herceptin and HER2/neu cancer markers (Fig. 21). These magnetic probes were successfully extended to the *in vivo* detection of cancer cells implanted in a mouse. When these WSIO–herceptin conjugates are intravenously injected into a mouse, they successfully reach and recognize HER2/neu receptors overexpressed from cancer cells. This results in a significant MR contrast effect in the tumor sites with a $\sim$20% decrease in $T2$ value compared to the control experiments (Fig. 22).

Heterostructured nanoparticles composed of magnetic and optical nanoparticles can further enable multimodal detection of biological targets. For example, Cheon, Shin, and co-workers fabricated "core–satellite" structured hybrid

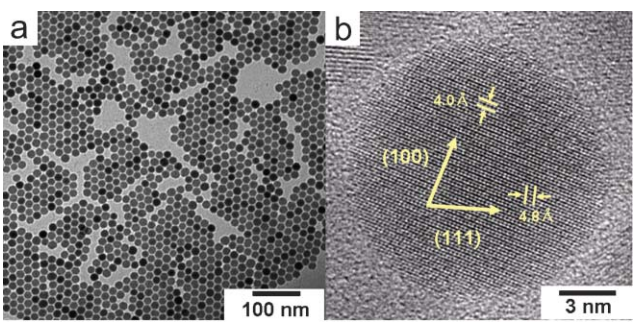

Fig. 20 (a) TEM and (b) HRTEM images of nonhydrolytically synthesized Fe_3O_4 nanoparticles.

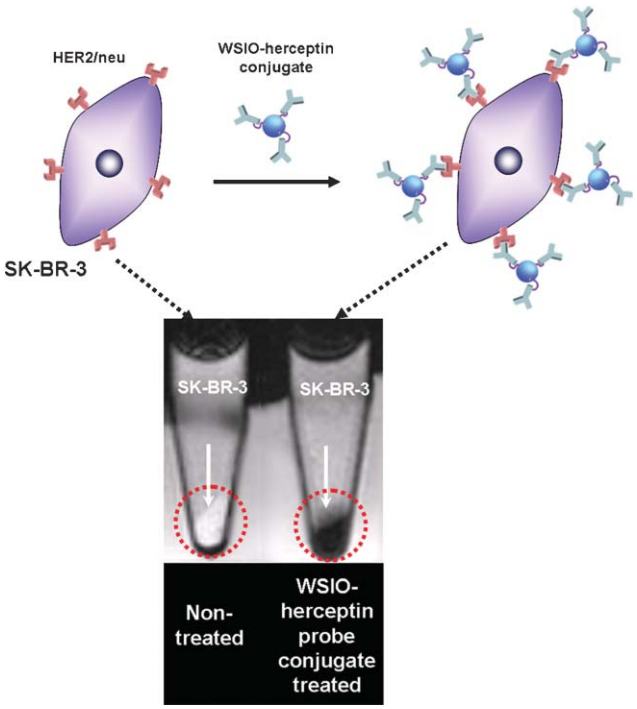

Fig. 21 Magnetic resonance cancer detection using Fe_3O_4–herceptin conjugates. Dark contrast in MR image was seen after the Fe_3O_4–herceptin conjugate treatment over SK-BR-3 cancer cells, which indicates successful targeting of the nanoparticle–antibody conjugates to HER2/neu cancer markers.[88]

nanoparticles comprised of a dye-doped silica "core" ($DySiO_2$) and multiple "satellites" of magnetic nanoparticles (Fe_3O_4) (Fig. 23(a), (b)).[90] Interestingly, they exhibited superior fluorescence and MR imaging capabilities, with as much as four times improvement, through the synergistic enhancement of its respective components. Further demonstration of their utilization for simultaneous optical and MR imaging of neuroblastoma cells expressing polysialic acids (PSAs) which is an important carbohydrate associated to neural markers was feasible. By conjugating the core–satellite nanoparticles with HmenB1 antibodies which specifically bind to the PSA (Fig. 23(c)), the resulting conjugates successfully detect PSA positive cells (CHP-134) with dark MR contrast in the *T*2*-weighted MR image (Fig. 23(d)). In addition, a strong red fluorescence was observed from the membrane regions of the CHP-134 cells (Fig. 23(e)). Since it is not possible to obtain such detailed cellular information from the MRI data alone, this result reflects that dual mode imaging is clearly advantageous in order to obtain both macroscopic (*e.g.* MRI) and microscopic sub-cellular (*e.g.* optical imaging) information of biological events.

4 Conclusions

As discussed in this article, multicomponent heterostructured magnetic nanoparticles possess unprecedented and enhanced nanoscale magnetic properties through synergistic interactions between the nanoparticle components as well as multifunctionalities due to properties of each of the individual components. Examples include magnetic alloy effects, nanoscale phase transition behaviors, and synergistic MR contrast effects in core–satellite structures as described in Sections 2 and 3.

Further utilization of newly developed magnetic nanoparticles with superior magnetism can potentially lead to the development of next generation magnetic nanodevices in informational and biological technologies. For example, the use of patterned magnetic superlattices with enhanced magnetic coercivity and addressable coordinates while retaining their small size could enable a terabits $inch^{-2}$ level of magnetic recording media. In addition, ultrasensitive imaging

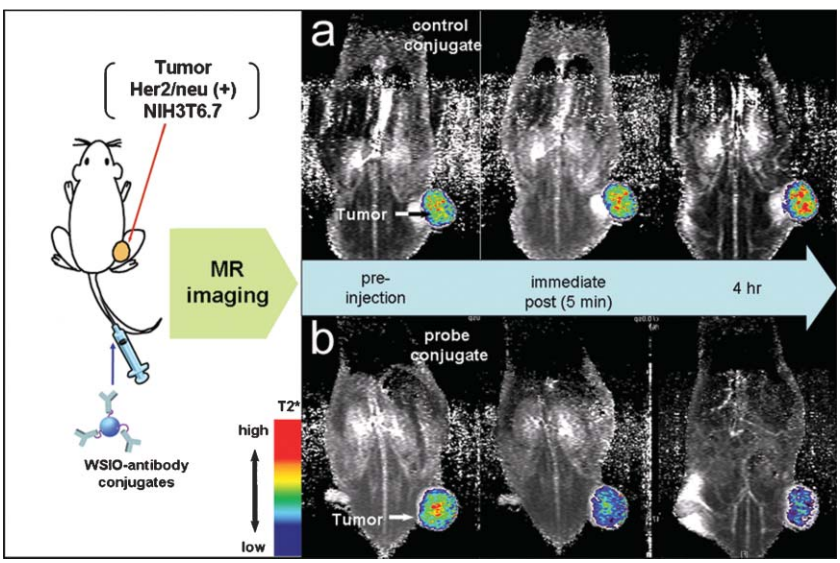

Fig. 22 *In vivo* cancer detection using Fe_3O_4–herceptin conjugates. Color maps of *T*2-weighted MR images of human breast cancer cell implanted in mice at the different temporal points (pre-injection, immediate post, 4 h) after the intravenous injection of (a) control conjugates and (b) WSIO–herceptin probe conjugates. Whereas negligible difference is seen in the color mapped MRI of a tumor site for the control conjugate, an immediate (5 min) color change from green to blue is evident with the probe conjugate, which corresponds to the ~20% decrease in *T*2 value.[89]

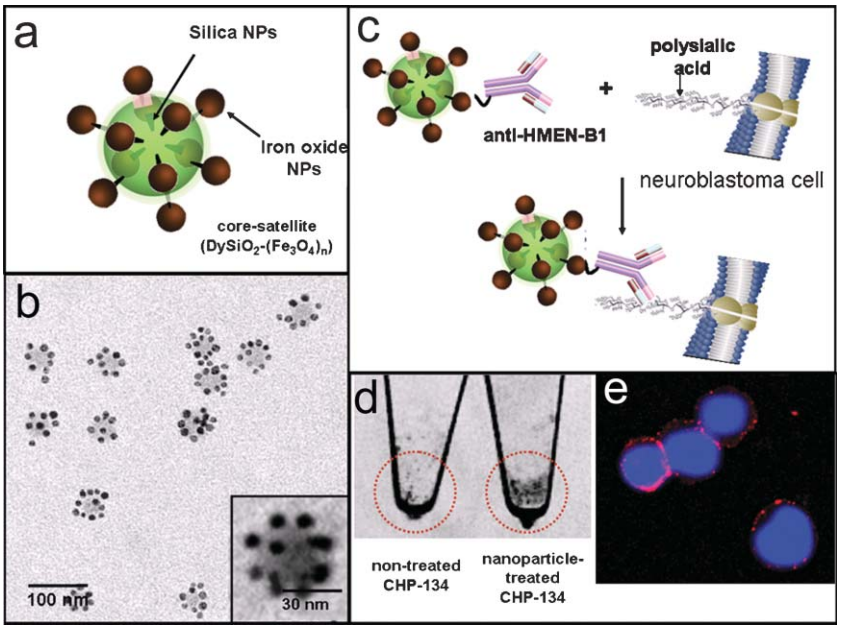

Fig. 23 Magnetic-optical dual-mode detection of polysialic acids (PSAs) expressed from neuroblastoma cells by using dye-doped silica ($DySiO_2$) core and multiple Fe_3O_4 satellite hybrid nanoparticles. (a) Schematic and (b) TEM image of $DySiO_2$–$(Fe_3O_4)_n$ core–satellite nanoparticles. (c) Schematic of molecular recognition of nanoparticle–antibody conjugates with PSAs. (d) MR and (e) optical detections of neuroblastoma.[90]

of biological events at the single/subcellular level can also be possible. The next step required for the success in this field is the development of more reliable and tailored synthetic protocols for the various types of heterostructured nanoparticles in conjunction with the required elucidation of new magnetic phenomena for their rapid implementation in a wide array of applications.

Acknowledgements

We would like to thank J.-g. Kim for HVEM analysis (KBSI), J.-M. Oh for TEM analyses (KBSI-Chuncheon), Dr O. H. Han and S. H. Kim for 9.4 T MRI (KBSI-Daegu). This work is supported in part by the National Research Laboratory (M10600000255), KRF (2004-041-C00186), and 2nd stage BK21.

References

1 D. Weller and A. Moser, *IEEE Trans. Magn.*, 1999, **35**, 4423.
2 K. Mohri, T. Uchiyama and L. V. Panina, *Sens. Actuators, A*, 1997, **59**, 1.
3 R. S. Molday and D. Mackenzie, *J. Immunol. Methods*, 1982, **52**, 353.
4 D. R. Baselt, G. U. Lee, M. Natesan, S. W. Metzger, P. E. Sheehan and R. J. Colton, *Biosens. Bioelectron.*, 1998, **13**, 731.
5 S. Goodwin, C. Peterson, C. Hob and C. Bittner, *J. Magn. Magn. Mater.*, 1999, **194**, 132.
6 Q. A. Pankhurst, J. Connolly, S. K. Jones and J. Dobson, *J. Phys. D*, 2003, **36**, R167.
7 F. J. Himpsel, J. E. Ortega, G. J. Mankey and R. F. Willis, *Adv. Phys.*, 1998, **47**, 511.
8 E. Katz and I. Willner, *Angew. Chem., Int. Ed.*, 2004, **43**, 6042.
9 G. Ozin and A. C. Arsenault, in *Nanochemistry*, Royal Society of Chemistry, Cambridge, UK, 1st edn, 2005.
10 D. L. Leslie-Pelecky and R. D. Rieke, *Chem. Mater.*, 1996, **8**, 1770.
11 B. D. Cullity, in *Introduction to Magnetic Materials*, ed. M. Cohen, Addison-Wesley, New York, 1st edn, 1972.
12 R. A. McCurrie, in *Ferromagnetic Materials: Structure and Properties*, Academic Press, New York, 1st edn, 1994.
13 J.-I. Park, N.-J. Kang, Y.-w. Jun, S. J. Oh, H. C. Ri and J. Cheon, *ChemPhysChem*, 2002, **3**, 543.
14 Z. F. Ren, Z. P. Huang, D. Z. Wang, J. G. Wen, J. W. Xu, J. H. Wang, L. E. Calvet, J. Chen, J. F. Klemic and M. A. Reed, *Appl. Phys. Lett.*, 1999, **75**, 1086.
15 M. Veith, A. Altherr, N. Lecerf, S. Mathur, K. Valtchev and E. Fritscher, *Nanostruct. Mater.*, 1999, **12**, 191.
16 B. Ning, M. E. Stevenson, M. L. Weaver and R. C. Bradt, *Surf. Coat. Technol.*, 2003, **163**, 112.
17 W. Lenggoro, Y. Itoh, N. Iida and K. Okuyama, *Mater. Res. Bull.*, 2003, **38**, 1819.
18 C. Janzen and P. Roth, *Combust. Flame*, 2001, **125**, 1150.
19 K. G. Paul, T. B. Frigo, J. Y. Groman and E. V. Groman, *Bioconjugate Chem.*, 2004, **15**, 394.
20 A. Cabanas and M. Poliakoff, *J. Mater. Chem.*, 2001, **11**, 1408.
21 J. G. Lee, J. Y. Park and C. S. Kim, *J. Mater. Sci.*, 1998, **33**, 3965.
22 M. Veith, M. Haas and V. Huch, *Chem. Mater.*, 2005, **17**, 95.
23 F. Torres, R. Amigo, J. Asenjo, E. Krotenko, J. Tejada and E. Brillas, *Chem. Mater.*, 2000, **12**, 3060.
24 O. Margeat, F. Dumestre, C. Amiens, B. Chaudret, P. Lecante and M. Respaud, *Prog. Solid State Chem.*, 2005, **33**, 71.
25 J. A. Lopez Perez, M. A. Lopez Quintela, J. Mira, J. Rivas and S. W. Charles, *J. Phys. Chem. B*, 1997, **101**, 8045.
26 X. Liu, Y. Guan, Z. Ma and H. Liu, *Langmuir*, 2004, **20**, 10278.
27 S. Sun, C. B. Murray, D. Weller, L. Folks and A. Moser, *Science*, 2000, **287**, 1989.
28 J.-I. Park and J. Cheon, *J. Am. Chem. Soc.*, 2001, **123**, 5743.
29 S. Sun, *Adv. Mater.*, 2006, **18**, 393.
30 E. V. Shevchenko, D. V. Talapin, A. L. Rogach, A. Kornowski, M. Haase and H. Weller, *J. Am. Chem. Soc.*, 2002, **124**, 11480.
31 X. Teng and H. Yang, *J. Am. Chem. Soc.*, 2003, **125**, 14559.
32 J.-I. Park, M. G. Kim, Y.-w. Jun, J. S. Lee, W.-r. Lee and J. Cheon, *J. Am. Chem. Soc.*, 2004, **126**, 9072.
33 S. U. Son, Y. Jang, J. Park, H. B. Na, H. M. Park, H. J. Yun, J. Lee and T. Hyeon, *J. Am. Chem. Soc.*, 2004, **126**, 5026.
34 W.-r. Lee, M. G. Kim, J.-r. Choi, J.-I. Park, S. J. Ko, S. J. Oh and J. Cheon, *J. Am. Chem. Soc.*, 2005, **127**, 16090.
35 N. S. Sobal, M. Hilgendorff, H. Mohwald, M. Giersig, M. Spasova, T. Radetic and M. Farle, *Nano Lett.*, 2002, **2**, 621.
36 X. Teng, D. Black, N. J. Watkins, Y. Gao and H. Yang, *Nano Lett.*, 2003, **3**, 261.

37 H. Kim, M. Achermann, L. P. Balet, J. A. Hollingsworth and V. I. Klimov, *J. Am. Chem. Soc.*, 2005, **127**, 544.
38 H. Zeng, J. Li, Z. L. Wang, J. P. Liu and S. Sun, *Nano Lett.*, 2004, **4**, 187.
39 J. Li, H. Zeng, S. Sun, J. P. Liu and Z. L. Wang, *J. Phys. Chem. B*, 2004, **108**, 14005.
40 W. Shi, H. Zeng, Y. Sahoo, T. Y. Ohulchansky, Y. Ding, Z. L. Wang, M. Swihart and P. N. Prasad, *Nano Lett.*, 2006, **6**, 875.
41 H. Yu, M. Chen, P. M. Rice, S. X. Wang, R. L. White and S. Sun, *Nano Lett.*, 2005, **5**, 379.
42 T. Pellegrino, A. Fiore, E. Carlino, C. Giannini, P. D. Cozzoli, G. Ciccarella, M. Respaud, L. Palmirotta, R. Cingolani and L. Manna, *J. Am. Chem. Soc.*, 2006, **128**, 6690.
43 Z. L. Wang, Z. R. Dai and S. Sun, *Adv. Mater.*, 2000, **12**, 1944.
44 H. Gu, R. Zheng, X. Zhang and B. Xu, *J. Am. Chem. Soc.*, 2004, **126**, 5664.
45 K.-W. Kwon and M. Shim, *J. Am. Chem. Soc.*, 2005, **127**, 10269.
46 H. Gu, Z. Yang, J. Gao, C. K. Chang and B. Xu, *J. Am. Chem. Soc.*, 2005, **127**, 34.
47 H. Gu, R. Zheng, H. Liu, X. Zhang and B. Xu, *Small*, 2005, **1**, 402.
48 G. H. Du, Z. L. Liu, Q. H. Lu, X. Xia, L. H. Jia, K. L. Yao, Q. Chu and S. M. Zhang, *Nanotechnology*, 2006, **17**, 2850.
49 S. Sun and C. B. Murray, *J. Appl. Phys.*, 1999, **85**, 4325.
50 V. F. Puntes, K. M. Krishnan and A. P. Alivisatos, *Science*, 2001, **291**, 2115.
51 F. Dumestre, B. Chaudret, C. Amiens, M.-C. Fromen, M.-J. Casanove, P. Renaud and P. Zurcher, *Angew. Chem., Int. Ed.*, 2002, **41**, 4286.
52 J. Osuna, D. de Caro, C. Amiens, B. Chaudret, E. Snoeck, M. Respaud, J.-M. Broto and A. Fert, *J. Phys. Chem.*, 1996, **100**, 14571.
53 D. L. Huber, *Small*, 2005, **1**, 482.
54 S. J. Park, S. Kim, S. Lee, Z. G. Khim, K. Char and T. Hyeon, *J. Am. Chem. Soc.*, 2000, **122**, 8581.
55 D. Farrell, S. A. Majetich and J. P. Wilcoxon, *J. Phys. Chem. B*, 2003, **107**, 11022.
56 X.-q. Li and W.-x. Zhang, *Langmuir*, 2006, **22**, 4638.
57 F. Dumestre, B. Chaudret, C. Amiens, P. Renaud and P. Fejes, *Science*, 2004, **303**, 821.
58 N. Cordente, M. Respaud, F. Senocq, M.-J. Casanove, C. Amiens and B. Chaudret, *Nano Lett.*, 2001, **1**, 565.
59 T. O. Ely, C. Amiens, B. Chaudret, E. Snoeck, M. Verelst, M. Respaud and J.-M. Broto, *Chem. Mater.*, 1999, **11**, 526.
60 J. Park, E. Kang, S. U. Son, H. M. Park, M. K. Lee, J. Kim, K. W. Kim, H.-J. Noh, J.-H. Park, C. J. Bae, J.-G. Park and T. Hyeon, *Adv. Mater.*, 2005, **17**, 429.
61 N. R. Jana, Y. Chen and X. Peng, *Chem. Mater.*, 2004, **16**, 3931.
62 J. Park, K. An, Y. Hwang, J.-G. Park, H.-J. Noh, J.-Y. Kim, J.-H. Park, N.-M. Hwang and T. Hyeon, *Nat. Mater.*, 2004, **3**, 891.
63 T. Hyeon, *Chem. Commun.*, 2003, 927.
64 S. Sun, H. Zeng, D. B. Robinson, S. Raoux, P. M. Rice, S. X. Wang and G. Li, *J. Am. Chem. Soc.*, 2004, **126**, 273.
65 J. Cheon, N.-J. Kang, S.-M. Lee, J.-H. Lee, J.-H. Yoon and S. J. Oh, *J. Am. Chem. Soc.*, 2004, **126**, 1950.
66 E. V. Shevchenko, D. V. Talapin, H. Schnablegger, A. Kornowski, O. Festin, P. Svedlindh, M. Haase and H. Weller, *J. Am. Chem. Soc.*, 2003, **125**, 9090.
67 K. Woo, J. Hong, S. Choi, H.-W. Lee, J.-P. Ahn, C. S. Kim and S. W. Lee, *Chem. Mater.*, 2004, **16**, 2814.
68 M. F. Casula, Y.-w. Jun, D. J. Zaziski, E. M. Chan, A. Corrias and A. P. Alivisatos, *J. Am. Chem. Soc.*, 2006, **128**, 1675.
69 Q. Song and Z. J. Zhang, *J. Am. Chem. Soc.*, 2004, **126**, 6164.
70 F. X. Redl, C. T. Black, G. C. Papaefthymiou, R. L. Sandstrom, M. Yin, H. Zeng, C. B. Murray and P. S. O'Brien, *J. Am. Chem. Soc.*, 2004, **126**, 14583.
71 M. Giersig and M. Hilgendorff, *Eur. J. Inorg. Chem.*, 2005, 3571.
72 H. Zeng, P. M. Rice, S. X. Wang and S. Sun, *J. Am. Chem. Soc.*, 2004, **126**, 11458.
73 V. Russier, C. Petit, J. Legrand and M. P. Pileni, *Phys. Rev. B*, 2000, **62**, 3910.
74 J. Schotter, P. B. Kamp, A. Becker, A. Puhler, D. Brinkmann, W. Schepper, H. Bruckl and G. Reiss, *IEEE Trans. Magn.*, 2002, **3365**, 28.
75 C.-H. Jun, Y. J. Park, Y.-R. Yeon, J. Choi, W.-r. Lee, S.-j. Ko and J. Cheon, *Chem. Commun.*, 2006, 1619.
76 H. Gu, P.-L. Ho, K. W. T. Tsang, L. Wang and B. Xu, *J. Am. Chem. Soc.*, 2003, **125**, 15702.
77 C. Xu, K. Xu, H. Gu, R. Zheng, H. Liu, X. Zhang, Z. Guo and B. Xu, *J. Am. Chem. Soc.*, 2004, **126**, 9938.
78 I. S. Lee, N. Lee, J. Park, B. H. Kim, Y.-W. Yi, T. Kim, T. K. Kim, I. H. Lee, S. R. Paik and T. Hyeon, *J. Am. Chem. Soc.*, 2006, **128**, 10658.
79 S. J. Son, J. Reichel, B. He, M. Schuchman and S. B. Lee, *J. Am. Chem. Soc.*, 2005, **127**, 7316.
80 D. Wang, J. He, N. Rosenzweig and Z. Rosenzweig, *Nano Lett.*, 2004, **4**, 409.
81 M. Kuhara, H. Takeyama, T. Tanaka and T. Matsunaga, *Anal. Chem.*, 2004, **76**, 6207.
82 G. X. Li, S. Sun, R. J. Wilson, R. L. White, N. Pourmand and S. X. Wang, *Sens. Actuators, A*, 2006, **126**, 98.
83 S. G. Grancharov, H. Zeng, S. Sun, S. X. Wang, S. O'Brien, C. B. Murray, J. R. Kirtley and G. A. Held, *J. Phys. Chem. B*, 2005, **109**, 13030.
84 A. Tsourkas, O. Hofstetter, H. Hofstetter, R. Weissleder and L. Josephson, *Angew. Chem., Int. Ed.*, 2004, **43**, 2395.
85 J. M. Perez, F. J. Simeone, Y. Saeki, L. Josephson and R. Weissleder, *J. Am. Chem. Soc.*, 2003, **125**, 10192.
86 R. Weissleder, A. Moore, U. Mahmood, R. Bhorade, H. Benveniste, E. A. Chiocca and J. P. Basilion, *Nat. Med.*, 2000, **6**, 351.
87 M. Lewin, N. Carlesso, C. H. Tung, X. W. Tang, D. Cory, D. T. Scadden and R. Weissleder, *Nat. Biotechnol.*, 2000, **18**, 410.
88 Y.-w. Jun, Y.-M. Huh, J.-s. Choi, J.-H. Lee, H.-T. Song, S. J. Kim, S. Yoon, K.-S. Kim, J.-S. Shin, J.-S. Suh and J. Cheon, *J. Am. Chem. Soc.*, 2005, **127**, 5732.
89 Y.-M. Huh, Y.-w. Jun, H.-T. Song, S. Kim, J.-s. Choi, J.-H. Lee, S. Yoon, K.-S. Kim, J.-S. Shin, J.-S. Suh and J. Cheon, *J. Am. Chem. Soc.*, 2005, **127**, 12387.
90 J.-H. Lee, Y.-w. Jun, S.-I. Yeon, J.-S. Shin and J. Cheon, *Angew. Chem., Int. Ed.*, 2006, **45**, 8160.
91 H. Zeng, J. Li, J. P. Liu, Z. L. Wang and S. Sun, *Nature*, 2002, **420**, 395.
92 J. Cheon, J.-I. Park, J.-s. Choi, Y.-w. Jun, S. Kim, M. G. Kim, Y.-M. Kim and Y. J. Kim, *Proc. Natl. Acad. Sci. USA*, 2006, **103**, 3023.
93 Q. A. Pankhurst, J. Connolly, S. K. Jones and J. Dobson, *J. Phys. D*, 2003, **36**, R167.
94 A. Jordan, R. Scholz, P. Wust, H. Fahling and R. Felix, *J. Magn. Magn. Mater.*, 1999, **201**, 413.

